ISSN 1063-7710, Acoustical Physics, 2023, Vol. 69, No. 1, pp. 30–39. © Pleiades Publishing, Ltd., 2023.
Russian Text © The Author(s), 2023, published in Akusticheskii Zhurnal, 2023, Vol. 69, No. 1, pp. 22–31.

NONLINEAR ACOUSTICS

Quasilinear Approximation for Modeling Difference-Frequency Acoustic Wave in a Diffracting Pump-Wave Beam

A. V. Tyurina[a], *, P. V. Yuldashev[a], I. B. Esipov[b], and V. A. Khokhlova[a]

[a] *Physics Faculty, Moscow State University, Moscow, 119991 Russia*

[b] *Gubkin Russian State University of Oil and Gas, Moscow, 119991 Russia*

**e-mail: tiurina.av@physics.msu.ru*

Received May 8, 2022; revised September 19, 2022; accepted September 22, 2022

Abstract—A quasilinear approach is considered to simulate generation of a difference-frequency acoustic wave by the interaction of two intense high-frequency diffracting pump beams with close frequencies. The boundary condition corresponds to dual-frequency excitation of an existing parametric source used for underwater research. It is shown that the linear field of primary waves has a high directivity with a total beam divergence angle of several degrees; therefore, the nonlinear-diffraction problem is solved numerically in the parabolic approximation. The pump wave field is calculated in the linear approximation; the solutions obtained at each step of the numerical grid along the beam axis are used to calculate nonlinear sources in the equation for a three-dimensional difference-frequency beam. The one- and two-dimensional distributions of the pressure field and the directivity pattern are analyzed for three values of a difference frequency. Numerical solutions obtained with realistic boundary conditions at the source and description of diffraction effects are compared with the known approximate analytical results for the quasilinear approach.

Keywords: difference frequency, quasilinear approach, diffraction

DOI: 10.1134/S1063771022700014

INTRODUCTION

Parametric processes of low-frequency wave generation remain a key area in modern acoustic research, which is associated with their important practical applications both in underwater acoustics for seawater tomography [1–3] and in aeroacoustics for generating highly directional audible sound in air [4–6].

Low-frequency wave is generated by the interaction of two high-frequency primary waves that are close in frequency. Such interaction is accompanied by a cascade process in which waves with new frequencies are formed. Since absorption of acoustic waves increases with frequency, the high-frequency components of the nonlinear wave field gradually attenuate as they propagate from the source, therefore at large distances, only a difference-frequency wave remains in the medium [7, 8]. The main disadvantage of such parametric excitation is the low-efficient energy conversion from pump waves into the difference-frequency wave; therefore, for a long time, this approach remained beyond the scope of practical applications. However, parametric effects have a number of significant advantages [9], such as the possibility of creating highly directional broadband sources of small wave sizes with suppressed sidelobes in their directivity patterns. Interest in this research area in underwater acoustics [3, 10] and aeroacoustics [11, 12] is still not decreasing.

When describing the processes of the generation and propagation of a difference-frequency wave, the one-way Westervelt equation serves as a sufficiently complete model [7, 13], which takes into account the effects of nonlinearity, diffraction, and thermoviscous absorption. This equation in the fully three-dimensional formulation can be solved numerically by the operator-splitting method [14, 15], in which for each operator in the numerical algorithm, its own finite-difference scheme is applied. In many practical problems, when calculating the fields of parametric sources, it is possible to use the paraxial approximation, and in this case, the simplified Khokhlov–Zabolotskaya–Kuznetsov (KZK) equation [16] is used. For modeling the KZK equation, effective numerical algorithms have been developed both in the frequency-domain, time-domain, and combined representations [17–20]. To calculate parametric sources, an entire class of approximate semianalytical solutions have been derived, which use additional approximations when setting the boundary conditions on the source and describing the beam divergence geometry, interaction length, and nonlinear and diffraction effects for the pump waves [21–23]. A wide range of models in this case uses the approximation of a given field of pump waves or the quasilinear theory [8, 24, 25].

In this study, the quasilinear approach is also used as a necessary step in developing a fully-nonlinear three-dimensional diffraction numerical model for the description of parametric interactions using the Westervelt and KZK equations. However, in this study, in contrast to the existing methods, a realistic boundary condition on the source is used for high-frequency pump waves, which corresponds to the operation of a recently developed underwater parametric array [26]. The generation of a difference-frequency wave in a free field is numerically modeled, taking into account the diffraction effects in both directions transverse to the preferred direction of wave propagation. Pump wave beams are calculated in the linear approximation; the solutions obtained at each step of the numerical grid along the beam axis are used to calculate nonlinear sources in the description of the three-dimensional difference-frequency field. The developed quasilinear approach is planned to be further extended to solve a three-dimensional fully-nonlinear diffraction problem using the optimized spectrum-filtering method developed in an earlier work by the authors, which can significantly reduce the number of operations in calculating the nonlinear operator [27].

THEORETICAL METHOD

Westervelt equation, which governs the directional propagation of a nonlinear acoustic wave, can be written in the retarded time coordinate system as [7]:

$$\frac{\partial^2 p}{\partial\tau\partial z} = \frac{c_0}{2}\left(\frac{\partial^2 p}{\partial x^2} + \frac{\partial^2 p}{\partial y^2} + \frac{\partial^2 p}{\partial z^2}\right) + \frac{\delta}{2c_0^3}\frac{\partial^3 p}{\partial\tau^3} + \frac{\beta}{2c_0^3\rho_0}\frac{\partial^2 p^2}{\partial\tau^2}, \tag{1}$$

where p is the acoustic pressure, z is the direction along the beam axis, $\tau = t - z/c_0$ is the retarded time, c_0 is the sound speed, ρ_0 is the density of the medium, and β and δ are the coefficients of nonlinearity and thermoviscous absorption in the medium, respectively.

In the case of linear propagation of a wave generated by a plane dual-frequency ultrasound source in a homogeneous medium with dissipation, the solution to linearized Westervelt equation (1) can be written as a Rayleigh integral [28, 29] with a complex value of the wavenumber $k_{1,2} = \omega_{1,2}/c_0 + ik''_{1,2}$:

$$P_{1,2}(\mathbf{r}) = -\frac{i\omega_{1,2}\rho_0}{2\pi}\int\frac{V^n_{1,2}(\mathbf{r}')e^{ik_{1,2}|\mathbf{r}'-\mathbf{r}|}}{|\mathbf{r}'-\mathbf{r}|}dS'_{1,2}, \tag{2}$$

where $P_{1,2}(\mathbf{r})$ are the complex pressure amplitudes of the pump waves; $p_{1,2} = ½P_{1,2}(\mathbf{r})\exp(-i\omega_{1,2}\tau)$ + c.c. is the distribution of the real pressure field with angular frequencies $\omega_{1,2} = 2\pi f_{1,2}$; $k_{1,2} = \omega_{1,2}/c_0 + ik''_{1,2}$ are the wavenumbers; $k''_{1,2}$ are the attenuation coefficients; $V^n_{1,2}(\mathbf{r}')$ are the complex amplitudes of the normal components of the vibrational velocity $v^n_{1,2} = ½V^n_{1,2}(\mathbf{r}')\times \exp(-i\omega_{1,2}\tau)$ + c.c. on the surface of the source; $\mathbf{r}'$ is the radius vector on the source surface; $\mathbf{r}$ is the radius vector at the observation point; $S'_{1,2}$ are the integration domains, which are the surfaces of the array's elements radiating at angular frequencies $\omega_{1,2}$ [26]. For a uniform distribution of the vibrational velocity, $V_n(\mathbf{r}') = v_0$ is the real value, where v_0 and $p_0 = v_0\rho_0c_0$ are characteristic amplitudes of the vibrational velocity and pressure at the source.

If the fields of high-frequency pump waves generated by the source considered here and calculated using the Rayleigh integral (2) has a high directivity with a total divergence angle in the far field of several degrees, as will be shown below, then the Westervelt equation (1) can be replaced by the nonlinear parabolic KZK equation, which is simpler for numerical solution [16]:

$$\frac{\partial^2 p}{\partial\tau\partial z} = \frac{c_0}{2}\left(\frac{\partial^2 p}{\partial x^2} + \frac{\partial^2 p}{\partial y^2}\right) + \frac{\delta}{2c_0^3}\frac{\partial^3 p}{\partial\tau^3} + \frac{\beta}{2c_0^3\rho_0}\frac{\partial^2 p^2}{\partial\tau^2}. \tag{3}$$

Following the quasilinear approach, we seek the solution to Eq. (3) by the successive approximations method [8, 24] in the form $p = p_A + p_B$, where $p_A = 1/2P_{\text{pump1}}(x, y, z)\exp(-i\omega_{\text{pump1}}\tau) + 1/2P_{\text{pump2}}(x, y, z)\exp(-i\omega_{\text{pump2}}\tau)$ + c.c. is the linear field of pump waves, which is the sum of two harmonic waves with frequencies $f_{\text{pump1}} = \omega_{\text{pump1}}/2\pi$ and $f_{\text{pump2}} = \omega_{\text{pump2}}/2\pi$ with complex pressure amplitudes $P_{\text{pump1}}(x, y, z)$ and $P_{\text{pump2}}(x, y, z)$; p_B is a small correction that includes the fields with new frequencies equal to the sum of the pump frequencies and their second harmonics, as well as the field of the difference-frequency wave $1/2P_{\text{dif}}(x, y, z)\exp(-i\omega_{\text{dif}}\tau)$ + c.c. with frequency $f_{\text{dif}} = |f_{\text{pump1}} - f_{\text{pump2}}| = \omega_{\text{dif}}/2\pi$. In this case, the complex pressure amplitudes of the pump waves satisfy the linear equation

$$\frac{\partial P_{\text{pump1,2}}}{\partial z} = \frac{ic_0}{2\omega_{\text{pump1,2}}} \times \left(\frac{\partial^2 P_{\text{pump1,2}}}{\partial x^2} + \frac{\partial^2 P_{\text{pump1,2}}}{\partial y^2}\right) - \frac{\delta\omega^2_{\text{pump1,2}}}{2c_0^3}P_{\text{pump1,2}}, \tag{4}$$

and the pressure amplitude of the difference-frequency wave satisfies the linear equation with the given source term:

$$\frac{\partial P_{\text{dif}}}{\partial z} = \frac{ic_0}{2\omega_{\text{dif}}}\left(\frac{\partial^2 P_{\text{dif}}}{\partial x^2} + \frac{\partial^2 P_{\text{dif}}}{\partial y^2}\right) - \frac{\delta\omega^2_{\text{dif}}}{2c_0^3}P_{\text{dif}} - \frac{i\beta\omega_{\text{dif}}}{2c_0^3\rho_0}P^*_{\text{pump2}}P_{\text{pump1}}. \tag{5}$$

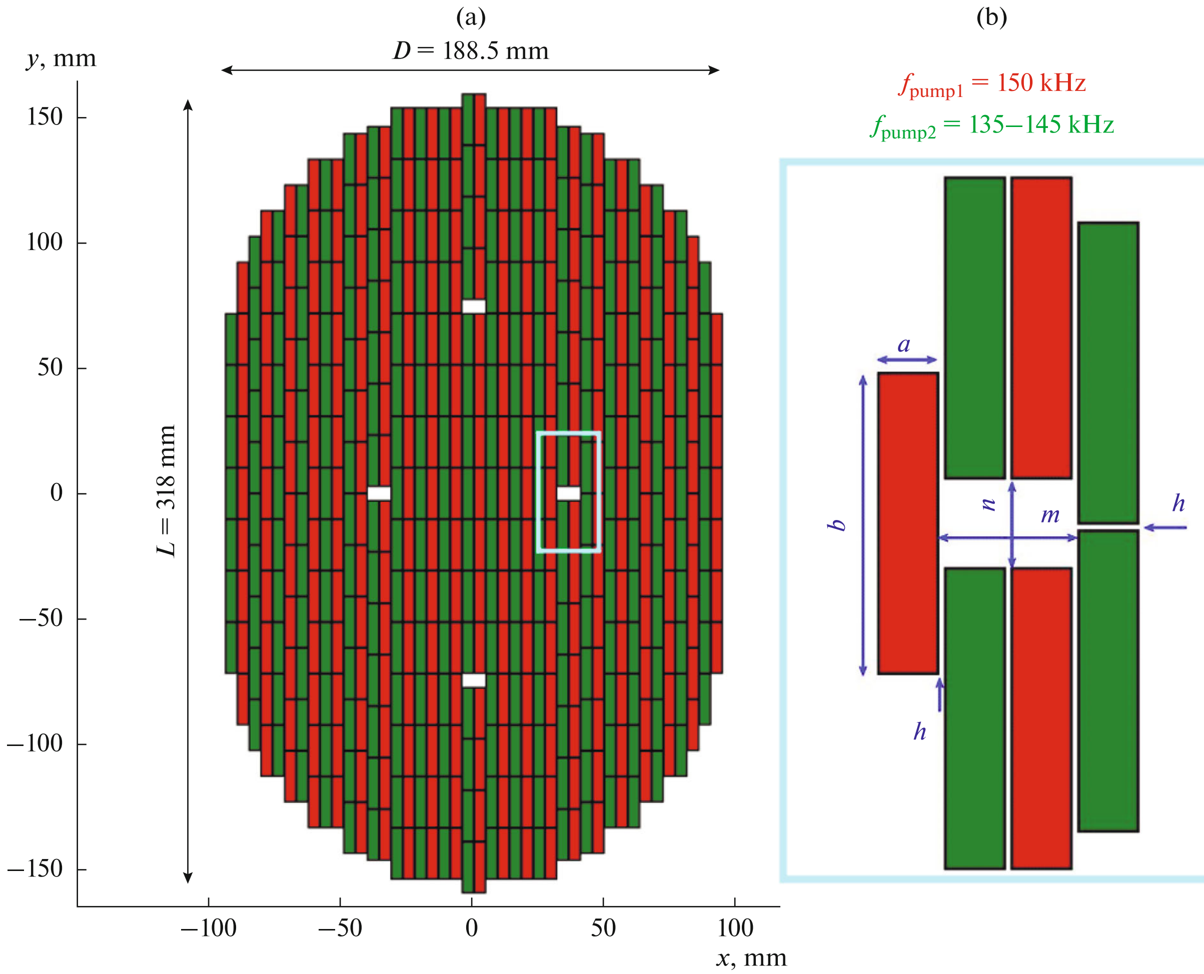

Fig. 1. (a) Geometry of ellipsoidal source with axes $L = 318$ mm and $D = 188.5$ mm with band structure radiating pump waves at two frequencies: fixed frequency $f_{\text{pump1}} = 150$ kHz (corresponding elements of source are marked in red) and varying frequency $f_{\text{pump2}} = 135–145$ kHz (corresponding elements of source are marked in green). The array consists of 544 elements with a size of $a \times b = 4 \times 20$ mm^2 and gap $h = 0.5$ mm between them and four inactive areas with a size $m \times n = 9.5 \times 6$ mm^2. (b) A diagram of the source near one of the inactive areas is shown.

BOUNDARY CONDITION

The difference-frequency wave field (5) was simulated using the parameters of a recently developed underwater parametric array (Fig. 1) with an ellipsoidal shape and a band structure of the surface distribution of radiating elements for channels with different frequencies [26]. Half of the rectangular elements operate at the fixed frequency $f_{\text{pump1}} = 150$ kHz; the other half—at a frequency varying from 135 to 145 kHz. The shape of the source is an ellipse with axes $L = 318$ mm vertically and $D = 188.5$ mm horizontally. The array consists of 544 elements with dimensions $a \times b = 4 \times 20$ mm^2, a gap $h = 0.5$ mm between the elements, and 4 inactive areas of $m \times n = 9.5 \times 6$ mm^2 size.

When calculating the Rayleigh integral (2) for each pump wave, at $z = 0$, we assumed the uniform distribution of the vibrational velocity components perpendicular to the element surfaces, i.e., directed along the z axis. However, since the boundary condition to the parabolic equations (4) and (5) was set for the complex pressure amplitude, the velocity distribution was recalculated to the pressure distribution as follows. First, the two-dimensional spatial spectrum $S_V(k_x, k_y)$ with spatial frequencies k_x and k_y in both transverse directions was calculated for a given uniform vibrational velocity distribution. Since the array is comprised of the identical rectangular elements, an analytical expression can be obtained for each rectangle: $S_{V,n}(k_x, k_y) = -ab/(4\pi^2)\text{sinc}(k_x a/2)\text{sinc}(k_y b/2)$, where n is the number of a rectangle, while the total spectrum $S_V(k_x, k_y)$ then can be calculated as the sum of contributions from individual elements, taking into account the geometry of their arrangement. The linearized Euler equation $\partial V/\partial t = (-1/\rho_0)\partial p/\partial z$ yields the relation between the distributions of the spatial spectra of the pressure and the z-component of the vibrational

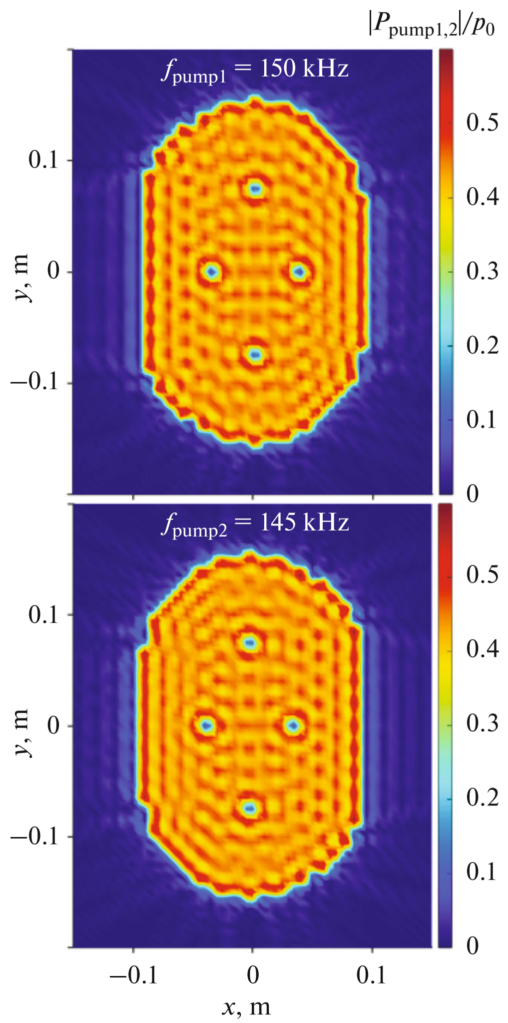

Fig. 2. Smoothed boundary conditions for normalized pressure amplitudes $|P_{\mathrm{pump}1,2}|/p_0$ on source for pump waves with frequencies $f_{\mathrm{pump}1}$ = 150 kHz and $f_{\mathrm{pump}2}$ = 145 kHz.

velocity of each rectangular element, $S_{P,n}(k_x, k_y) = \omega\rho_0 S_{V,n}(k_x, k_y)/(k^2 - k_x^2 - k_y^2)^{1/2}$, which allows for calculating the total spectrum $S_P(k_x, k_y)$. Then, the resulting boundary condition for the components of the angular spectrum $S_P(k_x, k_y)$ was filtered with a spatial filter that limits components with a spatial frequency higher than $0.7k_{\max}$, where $k_{\max}$ is the corresponding maximum wavenumber for each of the pump waves. Such filtering high spatial frequencies smooths out sharp gradients in the initial spatial pressure field distribution obtained using the inverse two-dimensional Fourier transform and reduces errors in the parabolic approximation when describing field components propagating at large angles with respect to the beam axis. Figure 2 shows the smoothened pressure amplitude distributions $|P_{\mathrm{pump}1,2}|/p_0$ of pump waves for frequencies $f_{\mathrm{pump}1}$ = 150 kHz and $f_{\mathrm{pump}2}$ = 145 kHz.

As the parameters of the medium and the value of the initial pressure, we used experimental data obtained for an underwater parametric array: $p_0 \le 0.6$ MPa, c_0 = 1502.25 m/s, ρ_0 = 996.81 kg/m^3 [26] and characteristic parameters of seawater: nonlinearity β = 3.5 and absorption $\delta = 4.42 \times 10^{-6}$ m^2/s [31]. It should be noted that in the experiment, for pressure amplitudes p_0 on the order of 0.6 MPa, nonlinear operation of the array was close to the shock formation regime, since the characteristic length of shock formation $l_{\mathrm{sh}} = \rho_0 c_0^3/(\beta\omega_{\mathrm{pump}1} p_0)$ in this case is 1.7 m [27], while the characteristic diffraction lengths for the array dimensions along the x and y axes are, respectively, $l_{d,x} = \omega_{\mathrm{pump}1,2}(D/2)^2/(2c_0)$ = 2.8 and 2.7 (2.6, 2.5) m, $l_{d,y} = \omega_{\mathrm{pump}1,2}(L/2)^2/(2c_0)$ = 7.9 and 7.7 (7.4, 7.1) m for pump waves with frequencies $f_{\mathrm{pump}1}$ = 150 kHz and $f_{\mathrm{pump}2}$ = 145 (140, 135) kHz. Therefore, to stay within the quasilinear approach, further simulation was carried out for the pressure amplitude p_0 = 0.06 MPa, which is ten times less than the maximum one achievable in the experiment.

NUMERICAL ALGORITHM

Let us consider three cases when the pump wave frequencies are multiples of the difference frequency and $f_{\mathrm{pump}1} > f_{\mathrm{pump}2}$, i.e. $f_{\mathrm{pump}1} = mf_{\mathrm{dif}}$ and $f_{\mathrm{pump}2} = (m-1)f_{\mathrm{dif}}$. Then, Eqs. (4), (5) for the complex pressure amplitudes of pump waves $P_{\mathrm{pump}1}(x, y, z)$, $P_{\mathrm{pump}2}(x, y, z)$ and the difference-frequency wave $P_{\mathrm{dif}}(x, y, z)$ are written as

$$\begin{cases} \dfrac{\partial P_{\mathrm{pump}1}}{\partial z} = \dfrac{ic_0}{2m\omega_{\mathrm{dif}}}\left(\dfrac{\partial^2 P_{\mathrm{pump}1}}{\partial x^2} + \dfrac{\partial^2 P_{\mathrm{pump}1}}{\partial y^2}\right) - \dfrac{\delta m^2\omega_{\mathrm{dif}}^2}{2c_0^3} P_{\mathrm{pump}1}, \\ \dfrac{\partial P_{\mathrm{pump}2}}{\partial z} = \dfrac{ic_0}{2(m-1)\omega_{\mathrm{dif}}}\left(\dfrac{\partial^2 P_{\mathrm{pump}2}}{\partial x^2} + \dfrac{\partial^2 P_{\mathrm{pump}2}}{\partial y^2}\right) - \dfrac{\delta (m-1)^2\omega_{\mathrm{dif}}^2}{2c_0^3} P_{\mathrm{pump}2}, \\ \dfrac{\partial P_{\mathrm{dif}}}{\partial z} = \dfrac{ic_0}{2\omega_{\mathrm{dif}}}\left(\dfrac{\partial^2 P_{\mathrm{dif}}}{\partial x^2} + \dfrac{\partial^2 P_{\mathrm{dif}}}{\partial y^2}\right) - \dfrac{\delta\omega_{\mathrm{dif}}^2}{2c_0^3} P_{\mathrm{dif}} - \dfrac{i\beta\omega_{\mathrm{dif}}}{2c_0^3\rho_0} P_{\mathrm{pump}1} P_{\mathrm{pump}2}^*. \end{cases} \tag{6}$$

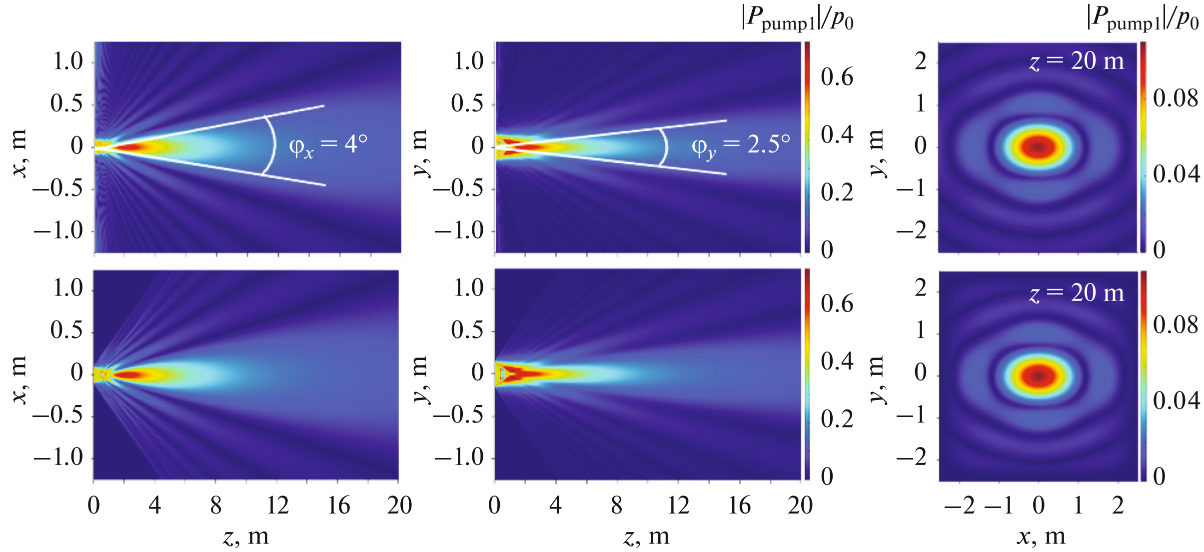

Fig. 3. Two-dimensional distributions of linear field of pump wave $|P_{pump1}|/p_0$ with frequency $f_{pump1} = 150$ kHz: top row, solution obtained with Rayleigh integral for ideal boundary conditions on source; bottom row, numerical solution of KZK equation with smoothed boundary conditions.

The first two equations of system (6) were solved at each grid step Δz by the above-mentioned operator-splitting method that ensured second-order accuracy of the numerical scheme for all three spatial coordinates:

$$P_{pump1,2}(x, y, z + \Delta z) = L_{D,\Delta z/2} L_{A,\Delta z} L_{D,\Delta z/2} P_{pump1,2}(x, y, z),$$

where the diffraction operator $L_{D,\Delta z/2}$ was calculated by the alternating-direction method [32], and for the absorption operator $L_{A,\Delta z}$, the exact solution in the form of a decaying exponent at a full grid step Δz was used. For the last equation of system (6), which describes the evolution of the amplitude of the difference-frequency wave, the numerical scheme was written as follows:

$$P_{dif}(x, y, z + \Delta z) = L_{D,\Delta z/2} L_{N,\Delta z/2} L_{A,\Delta z} L_{N,\Delta z/2} L_{D,\Delta z/2} P_{dif}(x, y, z), \quad (7)$$

where the diffraction and dissipative operators were calculated in a similar way, and the quasilinear operator $L_{N,\Delta z/2}$ was calculated by adding the function of nonlinear sources to the difference-frequency wave amplitude,

$$\frac{i\beta\omega_{dif}}{2c_0^3\rho_0} P_{pump1} P_{pump2}^*, \quad (8)$$

multiplied by a half-step $\Delta z/2$. Note that in the operator scheme (7), nonlinear sources at the first half-step $\Delta z/2$ were calculated as the arithmetic mean of the term (8), computed on the initial and intermediate layers, and at the second half-step $\Delta z/2$, on the intermediate and final layers.

RESULTS AND DISCUSSION

As a first step, the linear pressure fields of the pump waves were calculated using the Rayleigh integral (2). The top row in Fig. 3 shows an example of two-dimensional amplitude distributions $|P_{pump1}|$ of a wave with a frequency $f_{pump1} = 150$ kHz normalized to $p_0 = 0.06$ MPa. As follows from Fig. 3, the pump wave field has a high directivity with full beam divergence angles in the directions of the x and y axes of $\varphi_x = 4°$ and $\varphi_y = 2.5°$, respectively. Angles φ_x and φ_y were calculated at a level of 0.5 of the maximum amplitude using the corresponding one-dimensional transverse distributions obtained for $z = 20$ m and shown by the gray solid line in Figs. 4a and 4b. Thus, the pump wave field indeed has a small divergence, which makes it possible to use the parabolic approximation of Eq. (1), which is valid for components of the beam angular spectrum with full divergence angles up to 30° [30].

Figures 3 (bottom row) and 4 (red dashed line) show simulation results for the linearized KZK equation for the pressure amplitude of the pump wave with a frequency of 150 kHz versus the solution to the total diffraction model (Rayleigh integral). The inset to the axial pressure amplitude distribution along the z axis in Fig. 4c shows on an enlarged scale the behavior of both solutions in the near field of the beam. Clearly, numerical solution in the parabolic approximation hardly differs at all from the solution to exact diffraction problem (2), which confirms the validity of using the parabolic approximation and correctness of the numerical algorithm. Some differences, as expected, occur near the source up to distances of about 1 m, due to the influence and inaccurate description of the high-frequency components of the wave spatial spec-

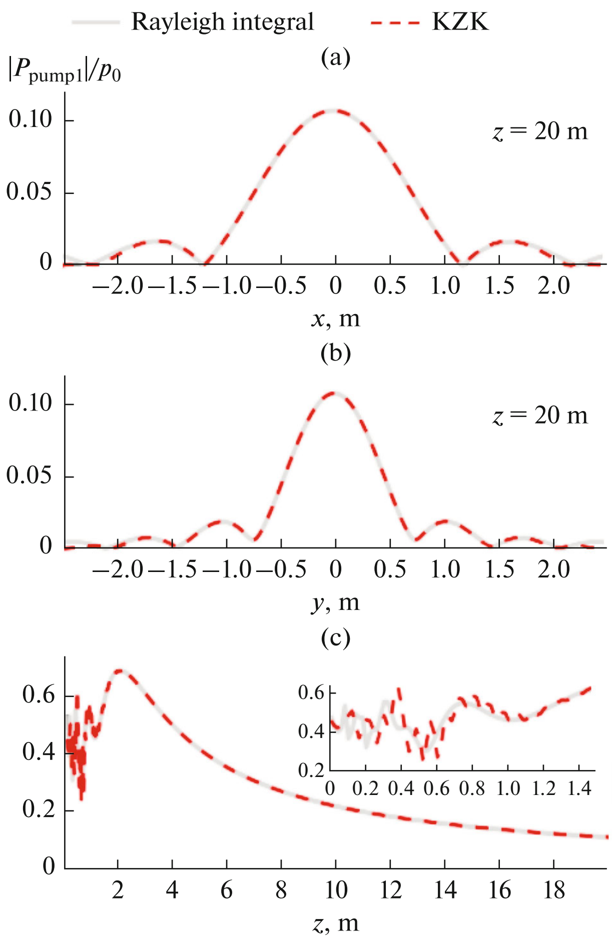

Fig. 4. One-dimensional distributions of pump wave amplitude $|P_{pump1}|/p_0$ with frequency $f_{pump1} = 150$ kHz: solid gray line, Rayleigh integral; red dashed line, numerical solution of KZK equation: (a, b) transverse distributions $|P_{pump1}|$ along x and y axes, calculated at distance $z = 20$ m; (c) axial distribution along z axis. Inset: solutions in near field.

trum in the near field of the beam at distances $z < a(ka)^{1/3}$, where k is the pump wavenumber and a is the characteristic size of the source [30].

For a pump wave with frequency $f_{pump1} = 150$ kHz, the pressure amplitude on the axis (Fig. 4c) reaches a maximum at a distance of about 2 m, which is smaller than the characteristic diffraction length $l_{d,x} = 2.8$ m for the shorter side of the array along the x coordinate, after which it decreases, asymptotically approaching the dependence $1/z$ according to the law of a divergent spherical wave. For pump waves with frequencies $f_{pump2} = 145$ (140, 135) kHz, the pressure field distributions have a similar form and are not given, since they differ only by a small—proportional to f_{dif}—decrease in amplitude in the far field at a distance $z = 20$ m by 3.2, 6.5, and 9.7%, respectively, due to the stronger divergence of beams with a lower frequency, as well as an insignificant—also proportional to f_{dif}—shift of the maximum in the axial pressure distribution by 3.1, 6.2, and 9.2% towards the source. It should be noted that, at the considered distances, the absorption effects have little effect for pump waves. The characteristic absorption length $l_{abs} = 2c_0^3/(\delta\omega^2)$ in seawater ($\delta = 4.42 \times 10^{-6}$ m^2/s [31]) for a frequency of 150 kHz is 1727 m, so the pressure amplitude of pump waves for $z = 20$ m is only 2% less, while at $z = 150$ m, 10% less than without absorption ($\delta = 0$). Thus, the effects of linear absorption of pump waves in this case will not limit the distance at which the pump wave energy is transferred to the difference frequency, i.e., the length of the end-fire array. Diffraction divergence effects are the only limiting factor for the quasilinear approach considered in this paper.

Figure 5 shows two-dimensional—normalized to $p_0 = 0.06$ MPa—distributions of the difference-frequency wave amplitude $|P_{dif}|$ for the case $f_{dif} = 5$ kHz, also demonstrating the high directivity of the difference-frequency wave field with full divergence angles $\varphi_x = 5.2°$ and $\varphi_y = 4.6°$ in the directions of the x and y axes, calculated similarly to pump waves at a level of 0.5 of the maximum amplitude using the corresponding one-dimensional transverse distributions (Figs. 6a, 6b) obtained for $z = 20$ m, and the absence of sidelobes, which is shown in more detail in Fig. 6.

Figures 6a and 6b show one-dimensional transverse distributions of the pressure amplitude of the difference-frequency wave $|P_{dif}|$ calculated in the far field of pump waves at a distance $z = 20$ m. These distributions were obtained for three values of the difference frequency $f_{dif} = 5$ (red curve), 10 (black curve), and 15 kHz (gray curve) and are normalized to np_0, where $n = 1$, 2, and 3, respectively. The field of considered difference-frequency waves is highly directional with total beam divergence angles of $\varphi_x = 5.2°$, 4.7°, 4.5° and $\varphi_y = 4.6°$, 4.0°, 3.7° in the direction of the x and y axes for $f_{dif} = 5$, 10, 15 kHz, which is somewhat wider than the similar directivity patterns of the pump waves. Clearly, the directivity of the difference-frequency wave increases with increasing f_{dif}, since the diffraction effects become weaker with increasing frequency. Note that for difference-frequency waves, the beam divergence angles in both directions differ less than for pump waves, since difference-frequency generation continues at distances larger than the diffraction length $l_{d,x}$ of pump waves, where high-frequency beams expand in this direction, but do not yet diffract in the direction of the y axis.

The dependences of the difference-frequency wave pressure amplitude along the beam axis are shown in Fig. 6c. At distances of up to 3 m, which are smaller than the diffraction length $l_{d,x}$ of a pump wave with respect to the x axis, for all three selected values of f_{dif}, the amplitude of the difference-frequency wave increases with distance z, since the amplitudes of pump waves are sufficiently large and their contribu-

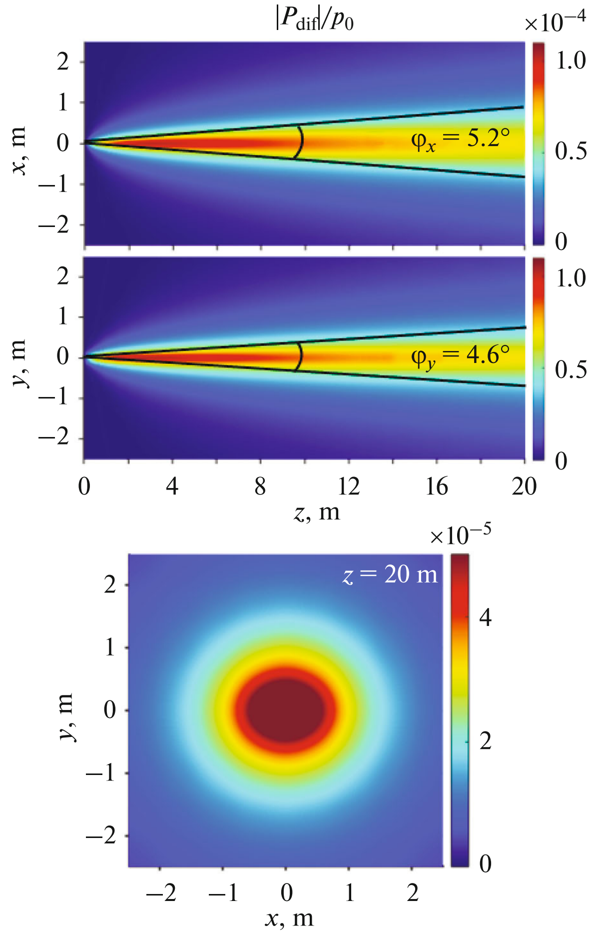

Fig. 5. Two-dimensional distributions of difference-frequency wave field $|P_{\rm dif}|$ with frequency $f_{\rm dif} = 5$ kHz, calculated in quasilinear approach and normalized to $p_0 = 0.06$ MPa.

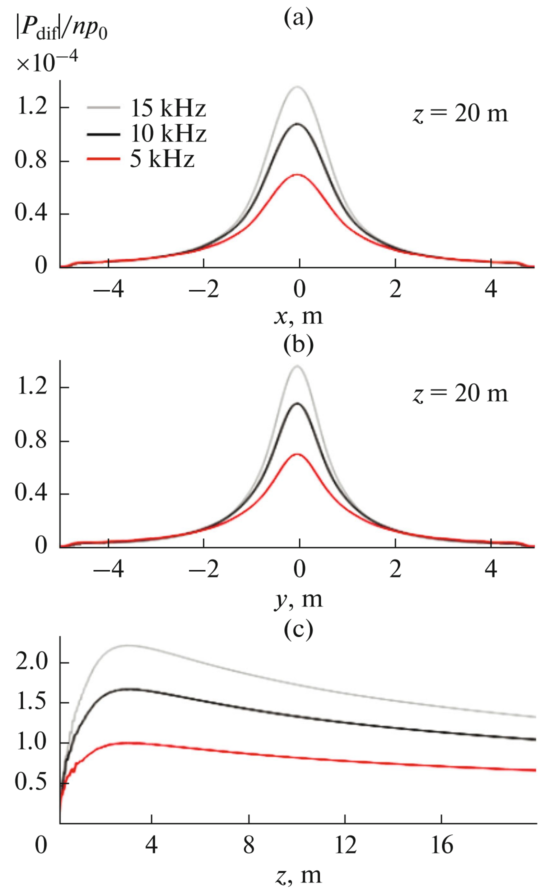

Fig. 6. Distributions of difference-frequency wave amplitude $|P_{\rm dif}|$, normalized to np_0, calculated for three cases of difference frequency $f_{\rm dif} = 5$ ($n = 1$, red line), 10 ($n = 2$, black line) and 15 kHz ($n = 3$, gray line) in quasilinear approach: (a, b) transverse distributions $|P_{\rm dif}|$ along x and y axes calculated at distance $z = 20$ m; (c) distribution along z axis.

tion to $p_{\rm dif}$ exceeds its decrease due to diffraction; then reaches a maximum at a distance of about 3 m, which is larger than for the pump waves, and gradually decreases, mainly due to diffraction effects, since, as mentioned above, dissipative losses for the physical values of the parameters of the medium are small. In addition, the amplitude of the difference-frequency wave also decreases due to a descent in the contribution from pump waves owing to a decrease in their amplitude resulting from the diffraction divergence of high-frequency beams.

Figure 6 shows that the higher the frequency $f_{\rm dif}$, the greater the maximum amplitude of the difference-frequency wave is, and it reaches 0.010, 0.034, and 0.069% of the pressure amplitude at the source p_0. In contrast to the plane wave approximation, where the amplitude of the difference-frequency wave is proportional to $f_{\rm dif}$, in the considered case of diffracting pump beams, it increases much faster than by a linear law due to weakening diffraction of a wave with a higher difference frequency. In this case, with an increase in pressure on the source, the efficiency of generating a difference-frequency wave, i.e., the dependence $|P_{\rm dif}|/p_0$ on p_0, enlarges linearly, which corresponds to the analytical results of the quasilinear approach [8].

Figure 7 shows the dependences of the difference-frequency wave amplitude, normalized to p_0, on the beam axis for the case $f_{\rm dif} = 5$ kHz and different distances from the source: the solid line shows the results of fully quasilinear calculation, and the various dashed lines show the dependences in the cases where sources (8) were artificially turned off when distances of $z = 8$, 12, 16 m (a), 50, 70, and 90 m (b) were reached. It follows from Fig. 7 that the generation of a difference-frequency wave continues at distances significantly exceeding the diffraction lengths of pump waves in both transverse directions, i.e., in spherically divergent beams of interacting waves, since a noticeable decrease in the pump wave amplitudes by e times will be observed only after the dissipation length is passed (the dissipation length of the pump waves is about 1700 m), which is many times greater than the diffrac-

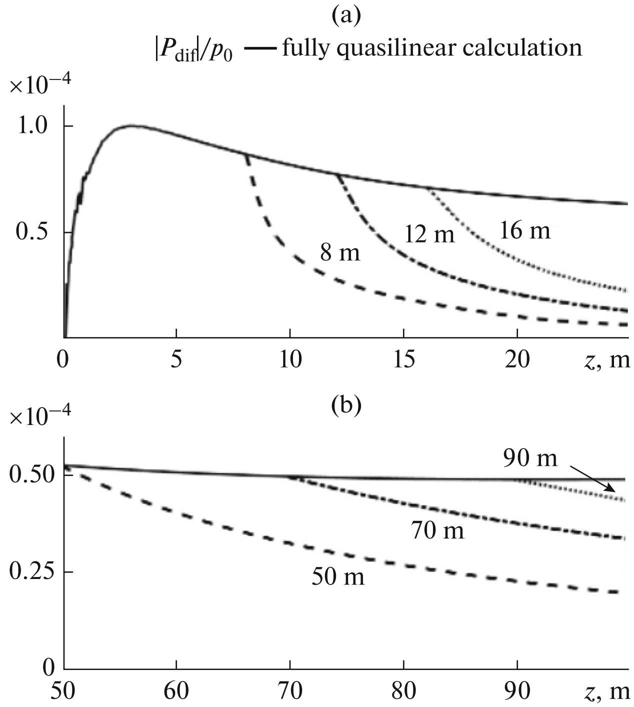

Fig. 7. Dependences of difference-frequency wave amplitude with $f_{dif} = 5$ kHz, normalized to $p_0 = 0.06$ MPa, along z axis: quasilinear calculation up to (a) z = 25 m and (b) 50 < z < 100 m (solid line) and with artificial switching-off of nonlinearity at various distances z = 8, 12, 16, 50, 70, 90 m (numbers next to curves).

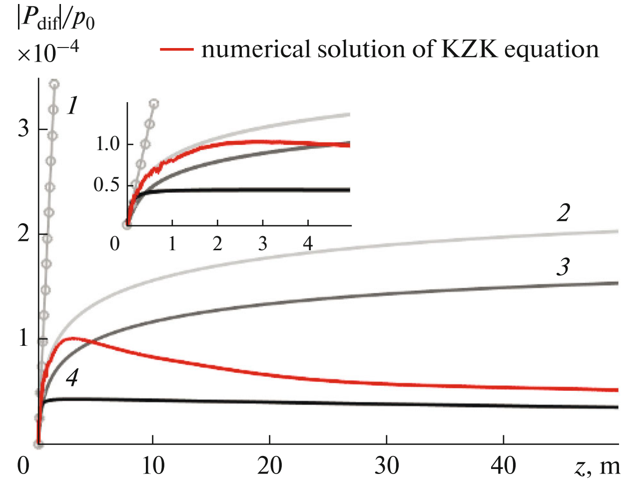

Fig. 8. Comparison of results of different quasilinear models for difference-frequency wave amplitude $f_{dif} = 5$ kHz on beam axis: numerical solution of KZK equation in quasilinear approach (red line) and approximate analytical models: calculation for plane waves (*1*), approximations of nondiffracting pump waves with initial Gaussian distribution on circular (*2*) and rectangular (*3*) sources, approximation of diffracting pump waves with initial Gaussian distribution on circular source (*4*). Inset: corresponding solutions in near field.

tion length; therefore, when sources are turned off at distances of at least up to $z = 90$ m, the difference-frequency wave amplitude begins to decay much faster. Thus, it should be expected that, as the amplitude of the pump waves increases and for numerical calculations without the quasilinear assumption, nonlinear effects of limiting the amplitudes of the pump waves due to cascading generation of higher harmonics would play an important role [22, 23].

Finally, it is of interest to compare the obtained results with those of existing approximate models that use the quasilinear approach, that is illustrated in Fig. 8 for the case $f_{dif} = 5$ kHz. The figure shows the dependences of the difference-frequency wave amplitude on the distance on the beam axis, obtained by various methods. The results of numerical solution of the KZK equation in the quasilinear approach are shown by red curves versus the results of four well-known analytical and semianalytical models. One of them calculates the difference-frequency wave amplitude under the assumption of plane pump wave interaction, so it increases limitlessly with increasing distance z [8]. The results of this model are shown in Fig. 8 by the gray line (Fig. 8, "*1*") and are only valid at distances $z \ll L_{d,x}, L_{d,y}$, where $L_{d,x} = 0.09$ m and $L_{d,y} = 0.26$ m are the diffraction lengths of the difference-frequency wave in both directions. Another model [8] assumes the interaction of nondiffracting pump waves with a Gaussian boundary distribution on a circular source of a radius $(S/\pi)^{1/2}$, where $S = 0.04352$ m^2 is the area of the array considered in the study. The results for this model are shown by the solid light gray line (Fig. 8, "*2*"); at small distances they correspond to the numerical solution of the KZK equation, but then the approximate solution continues to increase, since only diffraction of the difference-frequency wave is the limiting factor in it. The third model, shown by the solid dark gray line (Fig. 8, "*3*"), replicates the second one, but was obtained under the assumption of a rectangular source with dimensions corresponding to the L and D axes of the ellipse. This solution has been multiplied by an additional factor S/LD to compensate for the difference in the areas of the ellipsoid and rectangular sources and behaves similarly to model *2*. Finally, the fourth model takes into account diffraction of pump waves [8], which, like in the second model, have a Gaussian boundary distribution on a circular source with a radius $(S/\pi)^{1/2}$. The results for this model are shown in Fig. 8 by the solid black line (Fig. 8, "*4*") and have a similar trend with the numerical solution of the KZK equation obtained in this study: an initial increase in amplitude in the near field of the source and its slow decrease at large distances, in the zone of spherical divergence of the interacting waves. However, quantitatively, the results are very different, due to the difference in the boundary conditions on the source. Thus, all four analytical models correctly describe the behavior of the difference-frequency wave amplitude only in the near field on the beam axis but cannot be used at greater distances.

CONCLUSIONS

In this paper, numerical methods are used to study the three-dimensional diffraction problem of difference-frequency wave generation in the case of dual-frequency interaction of close high-frequency pump waves in the quasilinear approximation. The exact solution to the linear diffraction problem for pump waves using the Rayleigh integral was employed to demonstrate that the field of the initial waves has a high directivity; therefore, the KZK equation was then solved and the algorithm for calculating the diffraction operator in the parabolic approximation was used, the results of which barely differed from the solution to the exact diffraction problem.

In the quasilinear approach, one- and two-dimensional distributions of the difference-frequency wave amplitude are calculated for three different values of f_{dif}. It was shown that the directivity pattern of low-frequency radiation is wider and smoother in both transverse directions than for pump waves. In this case, the greater the value of the difference frequency, the higher directivity is of the beam generated by the parametric array.

The efficiency of generation of the difference-frequency wave field is analyzed as a function of f_{dif}, and it is shown that with an increase in the difference frequency, the portion of energy transferred into it from the pump waves increases. Thus, the difference-frequency wave amplitude increases by about 3.5 and 7 times with an increase in f_{dif} from 5 to 10 and 15 kHz, which differs from the plane wave approximation, where the amplitude of the difference-frequency wave increases linearly with increasing f_{dif}.

It was shown that, in the quasilinear approximation, the absorption and spherical divergence of interacting waves at the considered distances of ~100 m from the source are not the factors limiting the distances at which the difference-frequency beam is generated. Under realistic conditions on the source, when the pump wave amplitude increases and numerical calculations are performed without the quasilinear approximation, the nonlinear effects of decreasing pump wave amplitudes will play an important limiting role due to cascade generation of higher harmonics. An increase in the attenuation coefficient of seawater may also be a possible factor compared to the ideal case considered here due to the presence of particulate matter, algae, and other inclusions.

Comparison of the obtained numerical solution with the existing analytical results which were also derived with the quasilinear approach, but under additional assumptions about the boundary conditions on the source and behavior of high-frequency pump waves, showed that the analytical solutions yield a correct quantitative description of the behavior of the amplitude only in the near field of the source and only on the beam axis (model *4*), but they cannot be used for even a qualitative description of the field at larger distances.

The results obtained in this study provide the basis for further solving the fully-nonlinear three-dimensional diffraction problem of generating a difference-frequency wave with an array [26] in the case of more intense pump waves, when the quasilinear approach can no longer be applied.

FUNDING

The study was supported by the Russian Foundation for Basic Research (project no. 20-02-00676) and the BASIS Foundation (grant no. 20-2-2-21-1).

REFERENCES

1. B. K. Novikov and V. I. Timoshenko, *Parametrical Antennas in Hydrolocation* (Sudostroenie, Leningrad, 1990) [in Russian].
2. H. O. Berktay, J. Sound Vib. **2** (4), 435 (1965).
3. H. Zhou, S. H. Huang, and W. Li, Sensors **20** (7), 2148 (2020).
4. M. Yoneyama, J. Fujimoto, Y. Kawamo, and S. Sasabe, J. Acoust. Soc. Am. **73** (5), 1532 (1983).
5. C. Shi and W.-S. Gan, IEEE Potentials **29** (6), 20 (2010).
6. E. Skinner, M. Groves, and M. K. Hinders, Appl. Acoust. **148**, 423 (2019).
7. P. J. Westervelt, J. Acoust. Soc. Am. **35** (4), 535 (1963).
8. B. K. Novikov, O. V. Rudenko, and V. I. Timoshenko, *Nonlinear Underwater Acoustics* (Sudostroenie, Leningrad, 1981; AIP Publ., 1987).
9. O. A. Sapozhnikov, V. A. Khokhlova, R. O. Cleveland, P. Blanc-Benon, and M. F. Hamilton, Acoust. Today **15** (3), 55 (2019).
10. I. B. Esipov, K. A. Naugolnykh, and V. I. Timoshenko, Acoust. Today **6** (2), 20 (2010).
11. J. Pampin, J. S. Kollin, and E. Kang, in *Proc. Joint 33rd Int. Computer Music Conf.* (Copenhagen, 2007), p. 492.
12. J. Zhong, R. Kirby, and X. Qiu, J. Acoust. Soc. Am. **149** (3), 1524 (2021).
13. M. Cervenka and M. Bednarık, J. Acoust. Soc. Am. **146** (4), 2163 (2019).
14. J. Tavakkoli, D. Cathignol, R. Souchon, and O. A. Sapozhnikov, J. Acoust. Soc. Am. **104** (4), 2061 (1998).
15. R. J. Zemp, J. Tavakkoli, and R. S. C. Cobbold, J. Acoust. Soc. Am. **113** (1), 139 (2003).
16. M. A. Averkiou, Y.-S. Lee, and M. F. Hamilton, J. Acoust. Soc. Am. **94** (5), 2876 (1993).
17. S. I. Aanonsen, Tech. Rep. No. 73 (Dept. of Math., Univ. of Bergen, 1983).
18. Y. S. Lee and M. F. Hamilton, J. Acoust. Soc. Am. **97** (2), 906 (1995).

19. V. A. Khokhlova, R. Souchon, J. Tavakkoli, O. A. Sapozhnikov, and D. Cathignol, J. Acoust. Soc. Am. **110** (1), 95 (2001).
20. V. A. Khokhlova, A. E. Ponomarev, M. A. Averkiou, and L. A. Crum, Acoust. Phys. **52** (4), 481 (2006).
21. T. G. Muir and J. G. Willette, J. Acoust. Soc. Am. **52** (5), Part 2, 1481 (1972).
22. M. B. Moffett, R. H. Mellen, and W. L. Konrad, J. Acoust. Soc. Am. **61** (2), 325 (1977).
23. M. B. Moffett, R. H. Mellen, and W. L. Konrad, J. Acoust. Soc. Am. **63** (5), 1326 (1978).
24. M. Cervenka and M. Bednarik, J. Acoust. Soc. Am. **134** (2), 933 (2013).
25. D. Ding, J. Acoust. Soc. Am. **108** (6), 2759 (2000).
26. I. B. Esipov, O. E. Popov, and V. G. Soldatov, Acoust. Phys. **65** (4), 391 (2019).
27. A. V. Tyurina, P. V. Yuldashev, I. B. Esipov, and V. A. Khokhlova, Acoust. Phys. **68** (2), 130 (2022).
28. H. T. O'Neil, J. Acoust. Soc. Am. **21** (5), 516 (1949).
29. O. A. Sapozhnikov, S. A. Tsysar, V. A. Khokhlova, and W. Kreider, J. Acoust. Soc. Am. **138** (3), 1515 (2015).
30. J. N. Tjotta, S. Tjotta, and E. G. Vefring, J. Acoust. Soc. Am. **89** (3), 1017 (1991).
31. A. D. Pierce, *Acoustics: an Introduction to Its Physical Principles and Applications* (Springer, 2019).
32. W. H. Press, S. A. Teukolsky, W. T. Vetterling, and B. P. Flannery, *Numerical Recipes* (Cambridge Univ. Press, New York, 2007).